Environ Res Tec, Vol. 7, Issue. 3, pp. 335–346, September 2024

Environmental Research and Technology
https://ert.yildiz.edu.tr - https://dergipark.org.tr/tr/pub/ert
DOI: https://10.35208/ert.1432036

Environmental Research & Technology

Research Article

Radiation shielding and spectroscopic features of replacement materials: Reusing of agricultural and industrial wastes

Zeynep AYGÜN*[,1], Murat AYGÜN[2]

[1]*Vocational School of Technical Sciences, Bitlis Eren University, Bitlis, Türkiye*
[2]*Department of Physics, Bitlis Eren University, Faculty of Science and Arts, Bitlis, Türkiye*

ARTICLE INFO

Article history
Received: 05 February 2024
Revised: 02 March 2024
Accepted: 18 March 2024

Key words:
Agricultural wastes; Industrial waste; Radiation shielding; Phy-X/PSD

ABSTRACT

Environmental pollution increases due to the large amounts of waste production and raw material consumption depending on the increasing population. Agricultural and industrial wastes which are some of the sources of the pollution need to be reuse to reduce the negative impact on the environment and also contribute positive effect to the economy. In this context, industrial wastes such as clay types (red and green) and agricultural wastes such as egg shell, walnut shell and banana shell were used to prepare materials which can be used as replacement materials for construction industry. Radiation attenuation parameters (mass attenuation coefficients, effective atomic number, linear attenuation coefficients, mean free path, half-value layer, exposure and energy absorption build up factors, fast neutron removal cross-section) were acquired by Phy-X/PSD code. Spectroscopic techniques (XRD, EPR, SEM-EDS) were performed for the structural analysis. The existence of calcite main phase peaks (≈29.7) as well as SiO_2 (≈20° and 26°) and cellulose phases (≈16° and 34.7°) were observed by XRD. Mn^{+2} sextet lines with five weak doublets attributed to the forbidden transition lines of Mn^{+2} and a singlet with a g value of ≈2.00 and linewidth of ≈10 G were recorded by EPR. Among the samples, it was found that K1 (Red clay (20%)-eggshell waste (60%)-Bayburt stone waste (20%)), K3 (Red clay (60%)-eggshell waste (20%)-Bayburt stone waste (20%)), C3 (Red clay (60%)-eggshell waste (20%)-walnut shell waste (20%)) and Z3 (Green clay (60%)-egg shell waste (20%)-Bayburt stone waste (20%)) have the highest shielding potentials. All samples examined with good protection performances can be used as substitute materials instead of cement or aggregate for the aim of reusing the wastes and supporting the environmental and economic benefits.

Cite this article as: Aygün Z, Aygün M. Radiation shielding and spectroscopic features of replacement materials: Reusing of agricultural and industrial wastes. Environ Res Tec 2024;7(3)335–346.

INTRODUCTION

Climate change and global warming are among the current main environmental problems, and carbon dioxide emissions appear to be the main reason of these problems. As a natural result of the widespread concreting trend in the construction sector, among many sectors, the high cement production contributes to carbon dioxide emissions. Replacement materials using instead of cement are the research subjects of investigations around the world recently. Among these materials, wastes have a significant place in the studies. Clay types, ceramics, marble etc. which are generally thrown away as waste and known as construction material wastes can be reused or recycled to be used again as building materials. Replacing waste with common building materials to some extent has yielded positive results in

***Corresponding author.**
*E-mail address: zeynepyarbasi@hotmail.com

terms of durability and mechanical properties [1, 2]. Beyond on the industrial wastes, food wastes such as egg shell waste, banana shell waste and walnut shell wastes which are mostly consumed in our homes or in the food industry can be also evaluated for replacement. With the increasing population, environmental pollution also increases due to large amounts of waste production and raw material consumption. The storage situation of both agricultural waste and industrial waste is becoming an important problem, reaching a level that endangers public health. Such wastes need to be transformed into useful materials in order to reduce the negative impact on the environment and at the same time contribute to the economy [3]. Eggshell, marble dust and clay types are widely used and recycled wastes in engineering applications. Clay with refractory properties such as melting point, mechanical strength and thermochemical properties, has been preferred as one of the main building materials [4, 5]. Eggshell and marble dust which have nearly the same chemical contents (higher calcite amount) can be used as replacement instead of cement or aggregates. Since they have good pozzolanic and refractory properties, eggshell with high calcium (Ca) content and clay with high silicon (Si) percentage can make the mixture optimum for building materials.

In the recent years, due to the increase in radiation applications such as agriculture, scientific research, technology, industry, medical imaging and radiotherapy, information on protective measures against the harms of radiation has become valuable and interesting. In order to reduce radiation exposure, it is meaningful to obtain information on how much a building material reduces the transmission of gamma radiation. For this reason, the content of the material is important. Materials such as sand, cement, brick and concrete are also used with their protective properties as building materials. The radiation shielding features (RSF) of these materials can be developed by adding different components. In order to increase the performance of materials, environmentally friendly and lower cost resources can be developed by supplementing with natural materials and waste types. By reusing of wastes, it is possible to reduce environmental and economic problems. There is a great interest in researches involving radiation attenuation parameters that provide considerable information about the radiation shielding potentials (RSP) of materials [6–18]. These parameters are; mass attenuation coefficient, linear attenuation coefficient, mean free path, half value layer, one-tenth value layer, total atomic and electronic cross sections, effective atomic number, fast neutron removal cross section and buildup factors. In the study, the radiation attenuation parameters of developed new materials with clays, eggshell waste, walnut shell waste, banana shell waste mixtures were examined by the Phy-X/PSD program [19]. Thus, it is expected to determine whether the mixtures to be made are more advantageous in terms of shielding or not, and it is aimed to contribute to the literature with their spectroscopic properties and detailed analyzes. For this purpose, spectroscopic methods such as X-ray diffraction (XRD), electron paramagnetic resonance (EPR), energy dispersive spectroscopy (EDS) and scanning electron microscopy (SEM) were also performed for structural properties. Recycling more waste products such as eggshell, walnut shell waste, banana shell and utilizing environmental friendly products such as clay as additives for building materials can promote green and safer environment.

Table 1. The ratios (wt %) of the ingredients of the sample groups

Y group	Y1	Y2	Y3
GC-ESW-WSW	20-60-20	40-40-20	60-20-20
Z group	Z1	Z2	Z3
GC-ESW-BSW	20-60-20	40-40-20	60-20-20
K group	K1	K2	K3
RC-ESW-BSW	20-60-20	40-40-20	60-20-20
C group	C1	C2	C3
RC-ESW-WSW	20-60-20	40-40-20	60-20-20

GC: Green clays; ESW: Eggshell waste; WSW: Walnut shell waste; BSW: Banana shell waste.

MATERIALS AND METHODS

Sample Preparation

Four sample groups consisting of red and green clays (RC, GC), eggshell waste (ESW), banana shell waste (BSW) and walnut shell waste (WSW) were produced in different ratios and are given in Table 1. The elemental powders used in the manufacture of the alloys were mixed using a V-blender. Then, the element mixture to be pelletized was added to the mold with a diameter of 13 mm and a pressure of 8 MPa was applied.

Instrumentation

X-band JEOL JESFA300 EPR spectrometer with a 100 kHz and ≈9.2 GHz frequency was used for detecting room temperature EPR spectra of the alloys. 4 mm size samples were put in diamagnetic tubes for EPR measurements. XRD patterns were taken by BRUKER D8 ADVANCE X-ray diffractometer. X-ray diffractograms of the alloys were obtained with a scanning speed of 2.5°/min (40 kV and 40 mA) and radiation Cu-Kα (λ=1.54060 Å) in the range of 2Θ≈5°-90°. SEM images were recorded by ZEISS EVO LS10. EDS results were taken by JEOL JSM-6610 spectrometer.

Calculation Process

A recently developed Phy-X/PSD code is performed by entering the composition of the material as mole fraction or weight fraction. Density (g/cm^3) of the material knowledge is also necessary for obtaining the shielding parameters. A wide energy ranges 1 keV-100 GeV, some radioactive sources or some characteristic K-shell energies can be selected for performing the code. Parameters can be chosen depending on the purpose of the studies. The good feature of the code for obtaining the results is to get them in MS excel file.

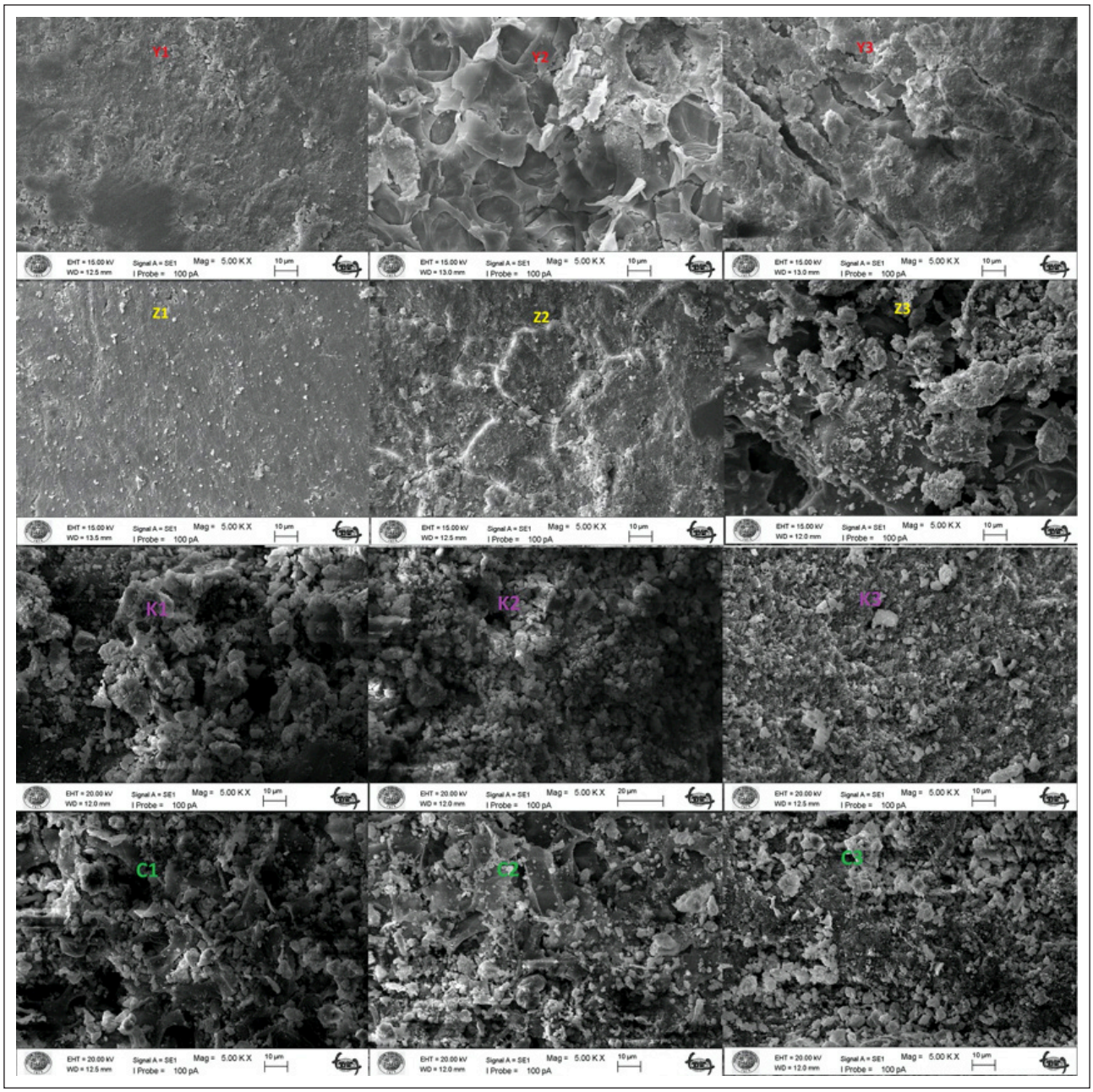

Figure 1. SEM images of the samples.

The mixture rule is used for the determination of density (ρ_{mix}) of the samples [20]:

$$\rho_{mix} = \frac{\sum_{i=1}^{n} c_i A_i}{\sum_{i=1}^{n} \frac{c_i A_i}{\rho_i}} \quad (1)$$

A_i, c_i and ρ_i, and are atomic fraction, atomic weight of element i_{th} and density, respectively.

The MAC can be determined based on the Beer–Lambert as:

$$I = I_0 e^{-\mu t} \quad (2)$$

$$\mu_m = \frac{\mu}{\rho} = ln(I_0/I)/\rho t = ln(I_0/I)/t_m \quad (3)$$

where t_m (g/cm^2), t (cm), μ(cm^{-1}) and μ_m(cm^2/g) are the sample mass thickness and thickness (the mass per unit area), LAC and MAC, respectively. MAC can be also acquired by Eq. 4 [21];

$$\mu/\rho = \sum_i w_i (\mu/\rho)_i \quad (4)$$

where w_i and $(\mu/\rho)_i$ and are the weight fraction and the MAC of the i_{th} constituent element, respectively.

MFP and HVL can be determined by the formulas,

$$MFP = \frac{1}{\mu} \quad (5)$$

$$HVL = \frac{In(2)}{\mu} \quad (6)$$

ACS (σ_a) and ECS (σ_e) can be calculated by the Eqs. 7, 8;

$$ACS = \sigma_a = \frac{N}{N_A}(\mu/\rho) \quad (7)$$

$$ECS = \sigma_e = \frac{\sigma_a}{Z_{eff}} \quad (8)$$

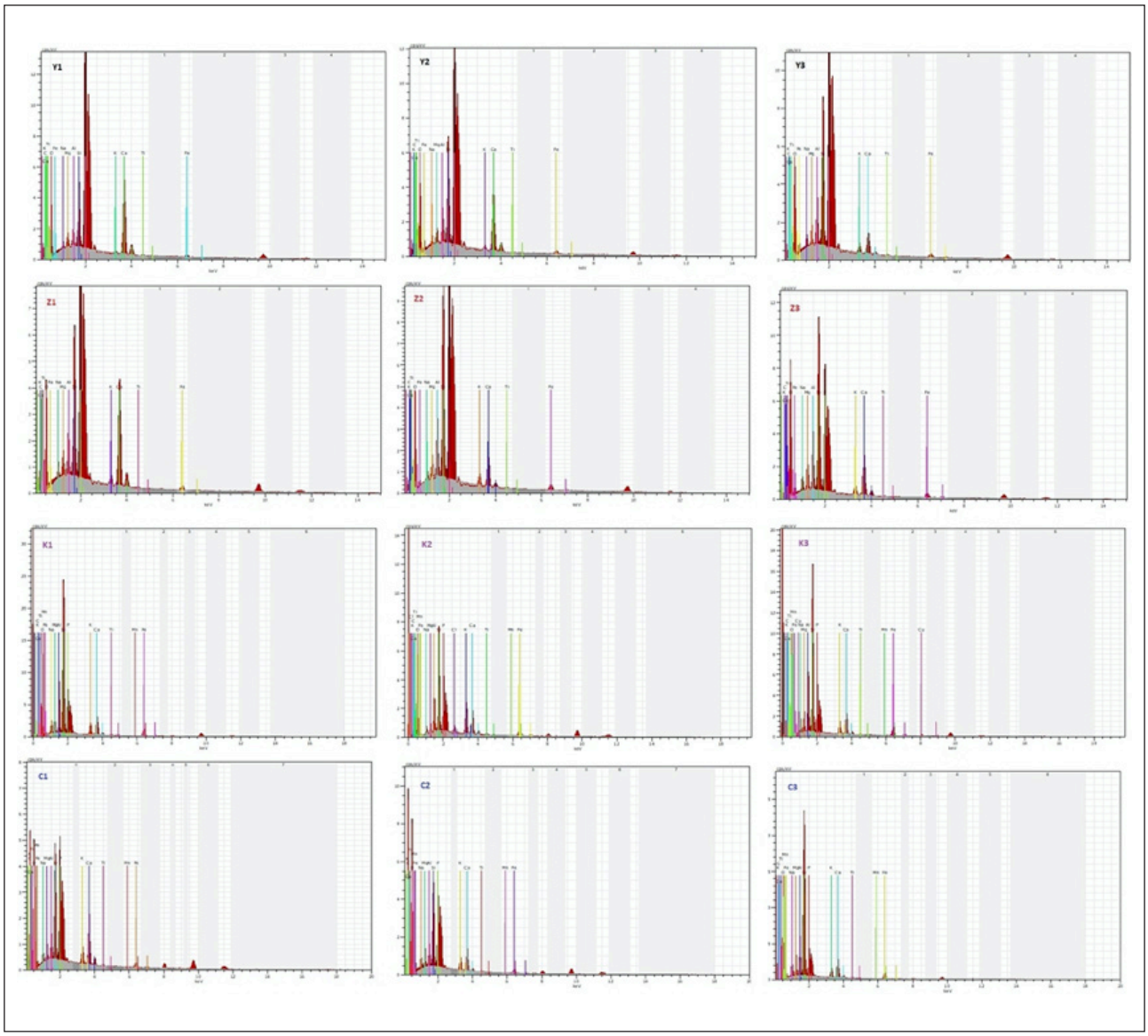

Figure 2. EDS results of the samples obtained by EDS.

Z_{eff} is found by the help of Eqs. (7) and (8) as;

$$Z_{eff} = \frac{\sigma_a}{\sigma_e} \quad (9)$$

Build up factors can be found by the equations given below [22, 23]. The geometric progression (G-P) fitting parameters is obtained by using values [24] in Eq. 14. EBF and EABF can be obtained using Eq. (12) or (13) by obtaining K(E, x) in Eq. (14), where x is thickness in mean free path (mfp) and a, b, c, d, X_k are the exposure GP fitting parameters. The ratio (R) of Compton partial MAC to total MAC should be defined for the material at specific energy. The R_1 and R_2 values indicate the $(\mu m)_{Compton}/(\mu m)_{Total}$ ratios of these two adjacent elements which have Z_1 and Z_2 atomic numbers. F_1 and F_2 are the values of G-P fitting parameters identical with the Z_1 and Z_2 atomic numbers at a certain energy, respectively. E and X demonstrate primary photon energy and penetration depth, respectively. Combination of K (E, X) with X, performs the photon dose multiplication and determines the shape of the spectrum [19].

$$Z_{eq} = \frac{Z_1(logR_2 - logR) + Z_2(logR - logR_1)}{logR_2 - logR_1} \quad (10)$$

$$F = \frac{F_1(logZ_2 - logZ_{eq}) + F_2(logZ_{eq} - logZ_1)}{logZ_2 - logZ_1} \quad (11)$$

$$B(E,x) = 1 + \frac{(b-1)(K^x - 1)}{(K-1)} \quad \text{for } K \neq 1 \quad (12)$$

$$B(E,x) = 1 + (b-1)x \quad \text{for } K = 1 \quad (13)$$

$$K(E,x) = cx^a + d\frac{\tanh\left(\frac{x}{X_k} - 2\right) - \tanh(-2)}{1 - \tanh(-2)} \quad \text{for } x \leq 40 \text{ mfp} \quad (14)$$

The FNRCS (ΣR) values of the samples are found as follows [19]:

$$\Sigma R = \Sigma_i \rho_i \left(\Sigma R/\rho\right)_i \quad (15)$$

where ρ_i and $\left(\Sigma R/\rho\right)_i$ are the partial density of the compound and the mass RCS of the ith constituent element, respectively.

Table 2. The weight (%) ratios of the elements obtained by EDS

Samples	O	C	Ca	K	Si	Na	Fe	Ti	Mg	P	Al	Mn	Density
Y1	70.02	12.75	5.59	0.11	1.81	0.29	0.49	0.1	0.39	7.96	0.51	–	1.563
Y2	71.74	11.54	4.37	0.17	2.86	0.38	0.68	0.07	0.41	6.93	0.84	–	1.570
Y3	68.59	16.82	1.20	0.36	3.43	0.42	0.63	0.09	0.55	6.87	1.05	–	1.587
Z1	66.10	15.32	5.72	0.34	3.07	0.50	0.74	0.07	0.55	6.66	0.93	–	1.583
Z2	73.32	10.52	1.77	0.40	4.14	0.30	0.97	0.10	0.55	6.72	1.21	–	1.586
Z3	57.60	4.40	6.71	1.25	10.97	1.25	2.34	0.19	1.85	9.85	3.60	–	1.684
K1	49.35	1.57	4.59	2.30	17.18	2.86	4.31	0.33	2.73	7.44	7.26	0.08	1.781
K2	71.34	12.61	2.10	2.22	4.14	0.55	1.60	0.10	0.42	2.95	1.57	0.09	1.559
K3	53.73	2.08	4.47	1.92	15.00	2.49	3.84	0.29	2.57	6.29	6.23	0.11	1.788
C1	61.64	23.51	3.29	1.10	2.90	0.86	0.68	0.08	0.63	3.98	1.24	0.07	1.574
C2	60.45	25.49	1.96	1.02	2.93	1.25	0.67	0.12	0.89	3.73	1.42	0.09	1.586
C3	51.37	1.44	4.40	1.93	17.01	3.73	3.78	0.29	2.86	5.45	7.59	0.16	1.760

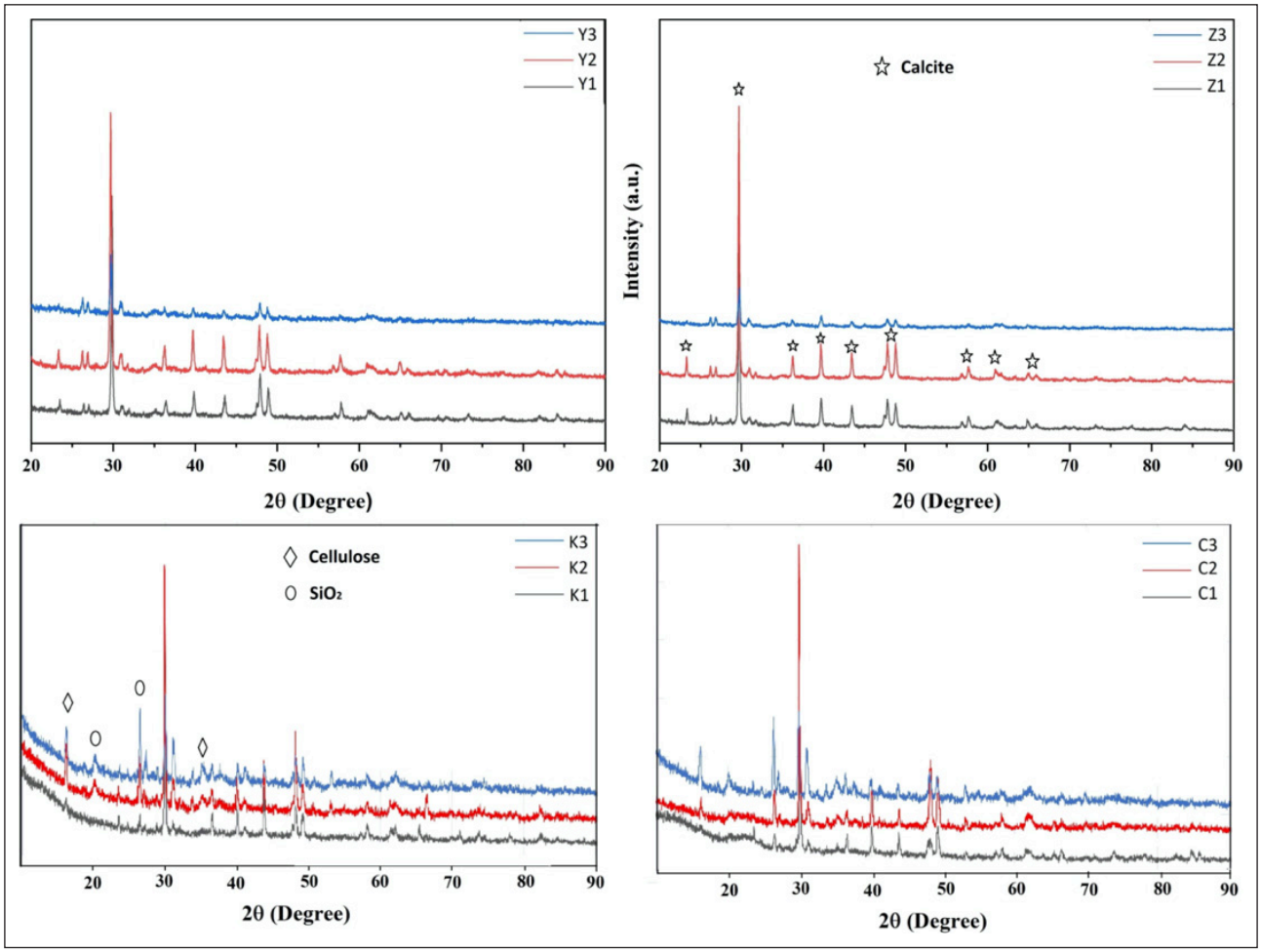

Figure 3. XRD patterns of the samples recorded at room temperature.

RESULTS AND DISCUSSION

SEM and EDS Analysis

SEM micrographs of the samples are given in Figure 1. Micro crystallites are observed for all samples in the SEM pictures. The smoothest surfaces are seen for Z1 and Y1 samples. The EDS spectra of the samples are given in Figure 2. The weight % ratios of the elements obtained from EDS are given in Table 2. It is understood from the EDS analyses that all the elements are common for all samples except from Mn. Y and Z groups do not have Mn element, while K and C groups have the element. This may be due to the device's limitations. The amount of Mn content of Y and Z groups samples may be lower than the others and so EDS cannot detect the element for the samples.

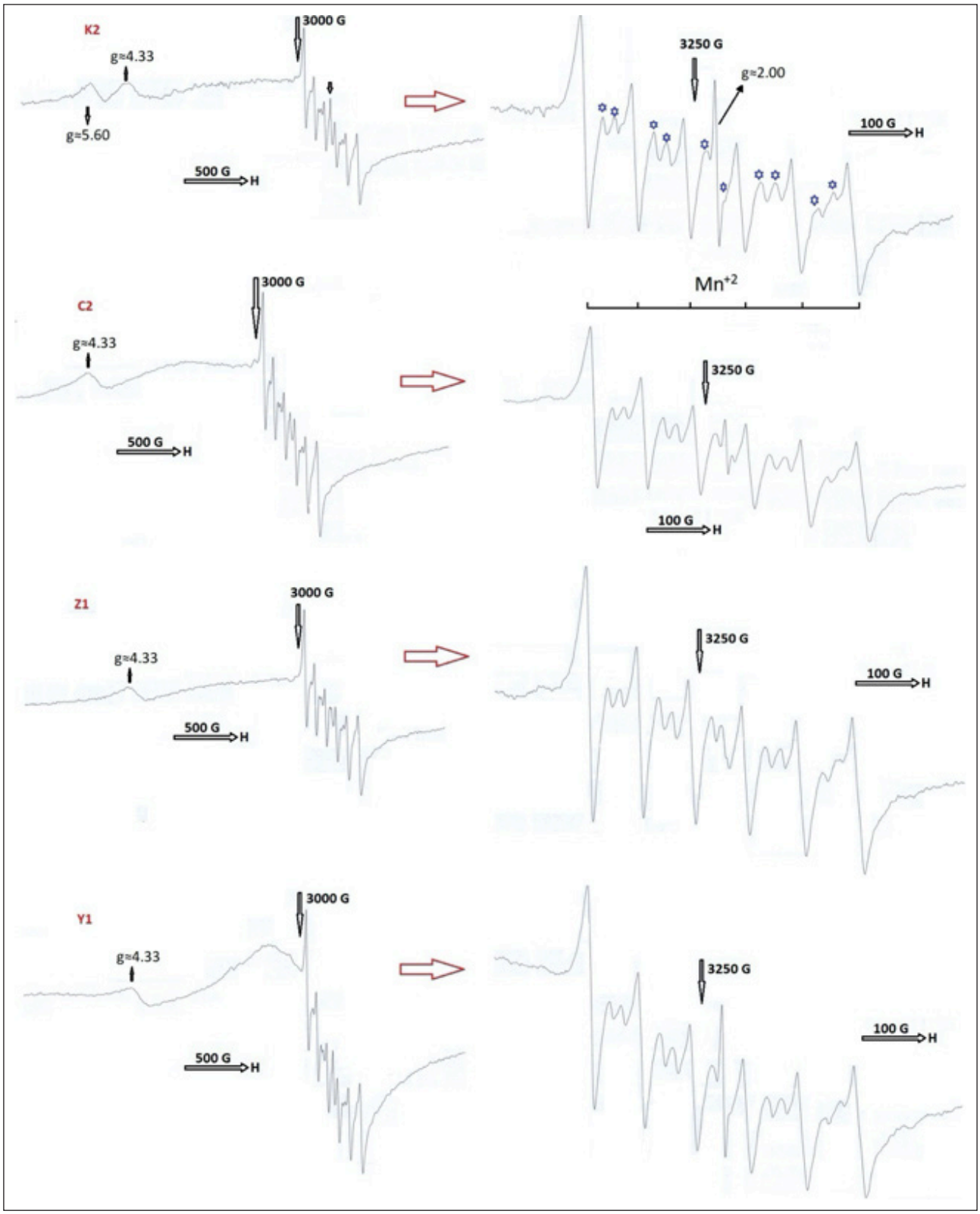

Figure 4. EPR spectra of the samples recorded by EPR.

XRD Analysis

Room temperature X-ray diffraction peaks are shown in Figure 3. The diffraction peaks were evaluated by the literature [25–28]. XRD results of the samples revealed the existence of $CaCO_3$ (calcite) main phase peak as well as SiO_2 and cellulose phases. The XRD peak obtained for all the samples at $2\theta \approx 29.7°$ is the characteristic crystalline structure of calcite ($CaCO_3$) [27]. The relatively broad XRD peak at the angle of ≈20° and 26° corresponds to the amorphous SiO_2 phase [25, 28]. The XRD peak at ≈16° and 34.7° is assigned to cellulose [25]. It is seen that diffraction peaks of the samples are generally calcite peaks, and also some peaks

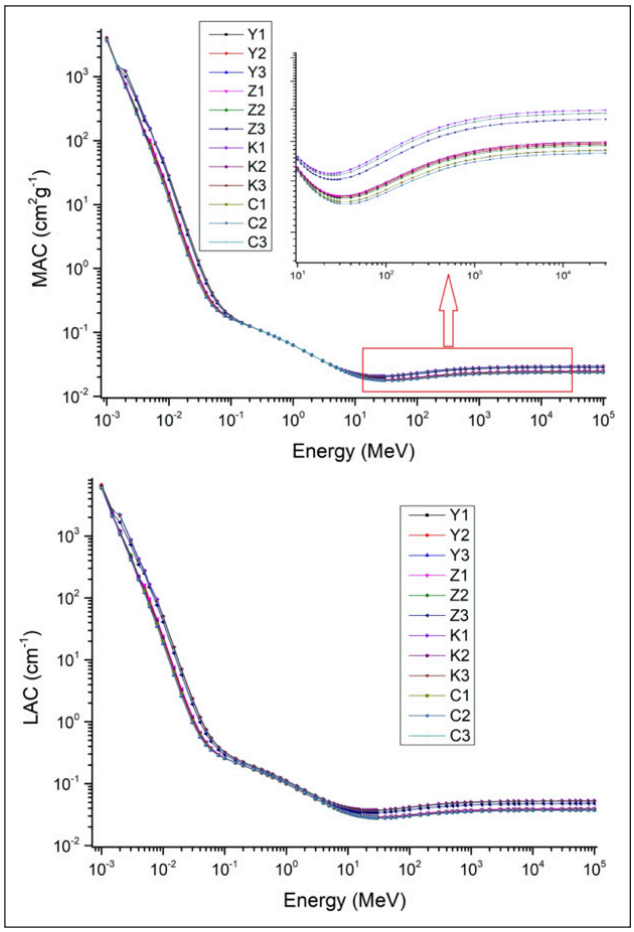

Figure 5. The variations of MAC and LAC versus photon energies.

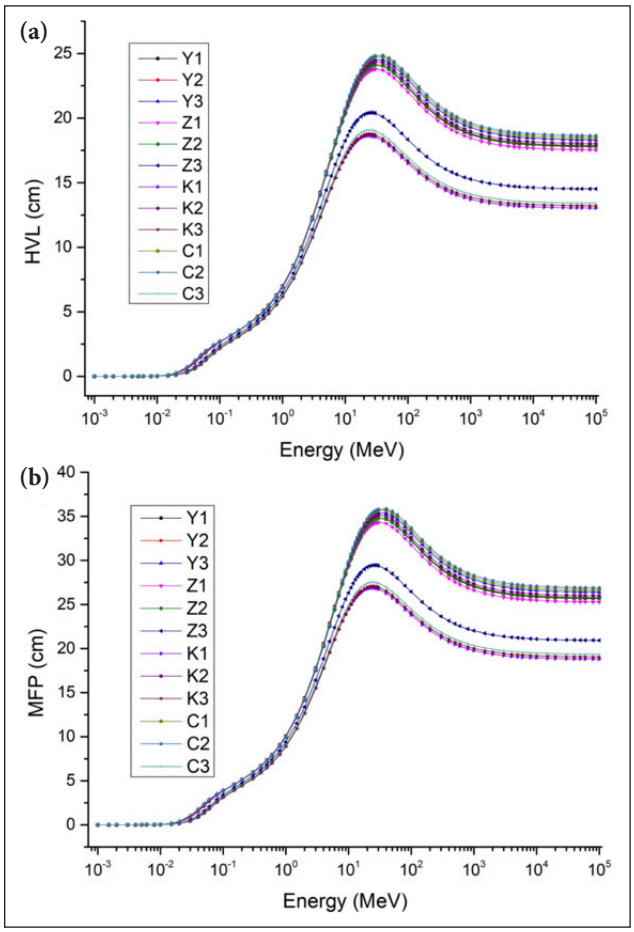

Figure 6. The variations of HVL **(a)** and MFP **(b)** versus photon energies.

of other phases are seen. This indicates that the samples are well crystallized.

The crystallite size for the evaluation of crystalline nature of the samples is determined by Debye-Scherer equation [29]. The full width half height (FWHM) for each diffraction can be used for this. λ is the X-ray wavelength, K is Scherer's constant and is of the order of ≅ 0.9, (β) is the FWHM in radians, d is the average size of the crystalline, and θ is the Bragg angle in degrees [30].

$$d=K\lambda/\beta\cos\theta \quad (1)$$

By using the FWHM of the most intense $CaCO_3$ peak (≈29.7°) of the samples, the crystallite sizes of $CaCO_3$ were found in the range of 33.0–63.3 nm.

EPR Study

Structures with paramagnetic centers can be detected by EPR technique in the existence of an external magnetic field. The EPR lines are defined by g-values by the equation of hυ = gβH. Here, β the Bohr magneton, h the Planck constant, H the magnetic field and υ the microwave frequency is used for the determination g values. Both in the crystalline nature and glassy phases, paramagnetic center affected by local magnetic fields centers can be acquired in EPR spectra. EPR spectra of the prepared samples recorded at room temperature are seen in Figure 4. For all group of samples, six hyperfine lines of Mn^{+2} (I=5/2) with g value of g≈2.00 is determined. It can be also detected that there is a weak a singlet (given by arrow) with a g value of ≈2.00 and linewidth of ≈10 G was obtained and overlapping with the Mn^{+2} lines. Additionally, five weak doublets which are attributed to the forbidden transition lines of Mn^{+2} (ΔmI=±1) are observed and marked by asterisks [25]. The g value obtained for the samples can be a result of organic free radical or a carbon centered organic radical [31–33].

Radiation Protection Analysis

Chemical composition (wt. %) of the samples acquired by EDS was used to obtain radiation-material interaction parameters by Phy-X/PSD code in the energy range of 1keV-100GeV. Changes of MAC values with incident photon energies are shown in Figure 5. The variations of MAC results are affected by photoelectric effect (PE) at low energies, Compton scattering (CS) at mid energies and pair production (PP) at high energies. The MAC values were also determined by XCom [34], and convenient results are obtained. The coherent results determined by both XCom and Phy-X/PSD are given in Table 3 for some of the energies at low, mid and high regions. The values demonstrated in blue color are the highest ones for MAC. LAC is the scattered or absorbed photon beam fraction per unit thickness. LAC values change with pho-

Table 3. MAC values of the samples obtained by Phy-X/PSD and XCom

Sample/code	2.0 x10^{-3} (MeV)	2.0 x10^{-2} (MeV)	2.0 x10^{-1} (MeV)	2.0 x10^{0} (MeV)	2.0 x10^{1} (MeV)	2.0 x10^{2} (MeV)	2.0 x10^{3} (MeV)
Y1 Phy-x/PSD	677.3	2.087	0.125	0.045	0.019	0.021	0.024
Y1 Xcom	677.2	2.087	0.124	0.044	0.018	0.021	0.024
Y2 Phy-x/PSD	714.3	1.994	0.125	0.044	0.019	0.021	0.025
Y2 Xcom	714.4	1.994	0.125	0.045	0.019	0.021	0.024
Y3 Phy-x/PSD	707.4	1.621	0.124	0.044	0.018	0.020	0.023
Y3 Xcom	707.4	1.621	0.124	0.044	0.018	0.020	0.023
Z1 Phy-x/PSD	710.3	2.175	0.125	0.044	0.019	0.021	0.024
Z1 Xcom	711.1	2.176	0.125	0.045	0.019	0.021	0.024
Z2 Phy-x/PSD	752.7	1.828	0.124	0.044	0.019	0.021	0.024
Z2 Xcom	752.8	1.828	0.124	0.044	0.019	0.021	0.024
Z3 Phy-x/PSD	986.0	3.380	0.126	0.044	0.020	0.024	0.028
Z3 Xcom	986.0	3.379	0.126	0.044	0.020	0.024	0.028
K1 Phy-x/PSD	1234.1	4.011	0.126	0.044	0.021	0.025	0.029
K1 Xcom	1234.0	4.011	0.126	0.044	0.021	0.025	0.029
K2 Phy-x/PSD	770.8	2.079	0.125	0.044	0.019	0.021	0.024
K2 Xcom	771.0	2.080	0.125	0.044	0.019	0.021	0.024
K3 Phy-x/PSD	1180.0	3.999	0.126	0.044	0.021	0.025	0.029
K3 Xcom	1180.0	3.999	0.126	0.044	0.021	0.025	0.029
C1 Phy-x/PSD	691.7	1.811	0.124	0.044	0.018	0.020	0.023
C1 Xcom	691.9	1.811	0.141	0.044	0.018	0.020	0.023
C2 Phy-x/PSD	693.9	1.644	0.124	0.044	0.018	0.020	0.023
C2 Xcom	693.8	1.644	0.124	0.044	0.018	0.020	0.023
C3 Phy-x/PSD	1248.4	3.757	0.126	0.044	0.021	0.025	0.029
C3 Xcom	1248.0	3.757	0.126	0.044	0.021	0.025	0.029

ton energies are shown in Figure 5. The LAC parameter varies as a function of MAC values and material density. Although the MAC and LAC values of the samples seem near, clearer results can be obtained with detailed analysis. The highest MAC values are found in the order of K1>K3>C3>Z3 and the lowest ones are that of Z2>C1>C2>Y3 among the samples.

The thickness halve the amount of incident photon energy is called as HVL and the average length traveled by a photon without scattering or absorption is called as MFP. Better shielding feature can be gained by the material with lower values of HVL and MFP. HVL and MFP values change with photon energies are shown in Figure 6. The values of HVL and MFP are in the order of K1<K3<C3<Z3<Z1<Y1<Z2<Y2<K2<Y3<C1<C2. So, the highest shielding performance is seen for K1 and the lowest one is for C2.

Z_{eff} is the average atomic number of material including more than one element. Z_{eff} values as a function of photon energy is shown in Figure 7. The highest Z_{eff} values are found at low energies based on the PE cross-section with the effect of Z^{4-5}. At mid-energies, a decrease is seen due to the CS cross-section changed with $E^{-3.5}$. At high energies, the PP

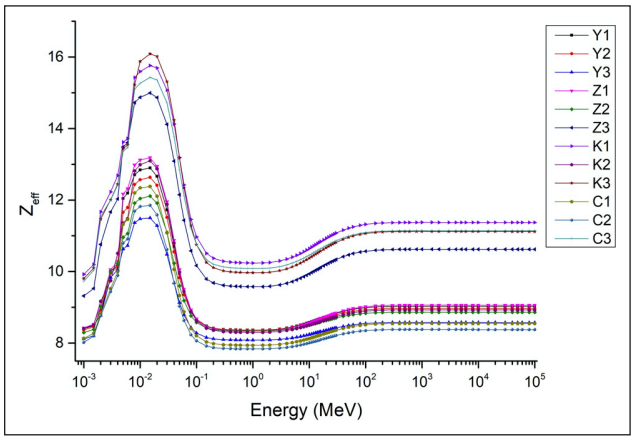

Figure 7. The variations of MAC and LAC versus photon energies.

cross-section variation changed with Z^2 causes an increase and then a stable case [30]. The presence of different atomic numbers in the material is effective on the variation of Z_{eff} values. As a result of this, samples with more than one element and large atomic number differences have larger fluctuations in Z_{eff} values (such as C-6; Fe-26). Among the

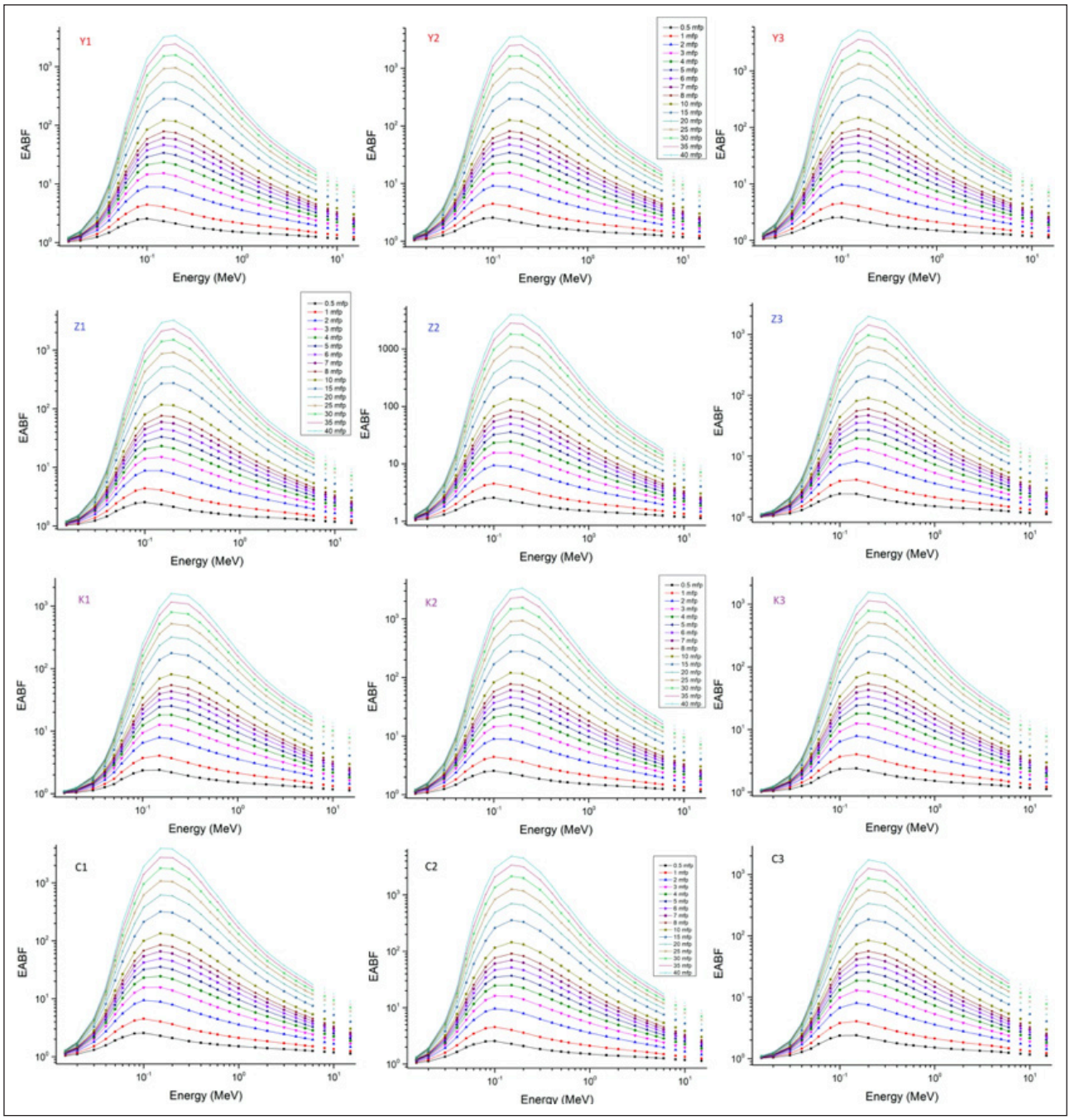

Figure 8. The changes of EABF of the samples versus photon energies.

samples, K1, K3, C3, Z3 and Y1 with higher Fe and Ca content have the higher Z_{eff} values. It is obtained that RSP of K1, K3, C3, Z3 and Y1 are higher based on Z_{eff} values.

Build up factor is expressed as the ratio of the total radiation at a given point to amount of uncollided radiation at the same point. EABF, one of the buildup factors, is related with the energy absorbed or deposited in the interacting material. EBF, the other one, is about the exposure in interacting material. Build up factors can be estimated as a function of mfp, and EBF and EABF values as a function of photon energies are given in Figures 8, 9. Buildup factor values are lower (due to the PE), the highest values (due to the large number of scattered photons by the CS) and lower again (due to the PP effect and strong photon absorption) in the low, mid and high energy regions, respectively [35]. Photon scattering and the probability of penetration depth related closely causes the buildup effect intensely at mid-energies. When the obtained buildup factors are analyzed, it is found that the photon accumulation, so the CS process is more for Y3 and C2 than the other samples, while that is less for K1 and K3.

Fast neutron attenuation capabilities of the samples were also obtainable by Phy-X/PSD and the cross sections are given in Figure 10. It is obtained that FNRCS value is the highest for C2 and that is the lowest for Z3 among the samples. It is possible to note that the samples C2 with lower photon shielding capability has higher neutron shielding capability.

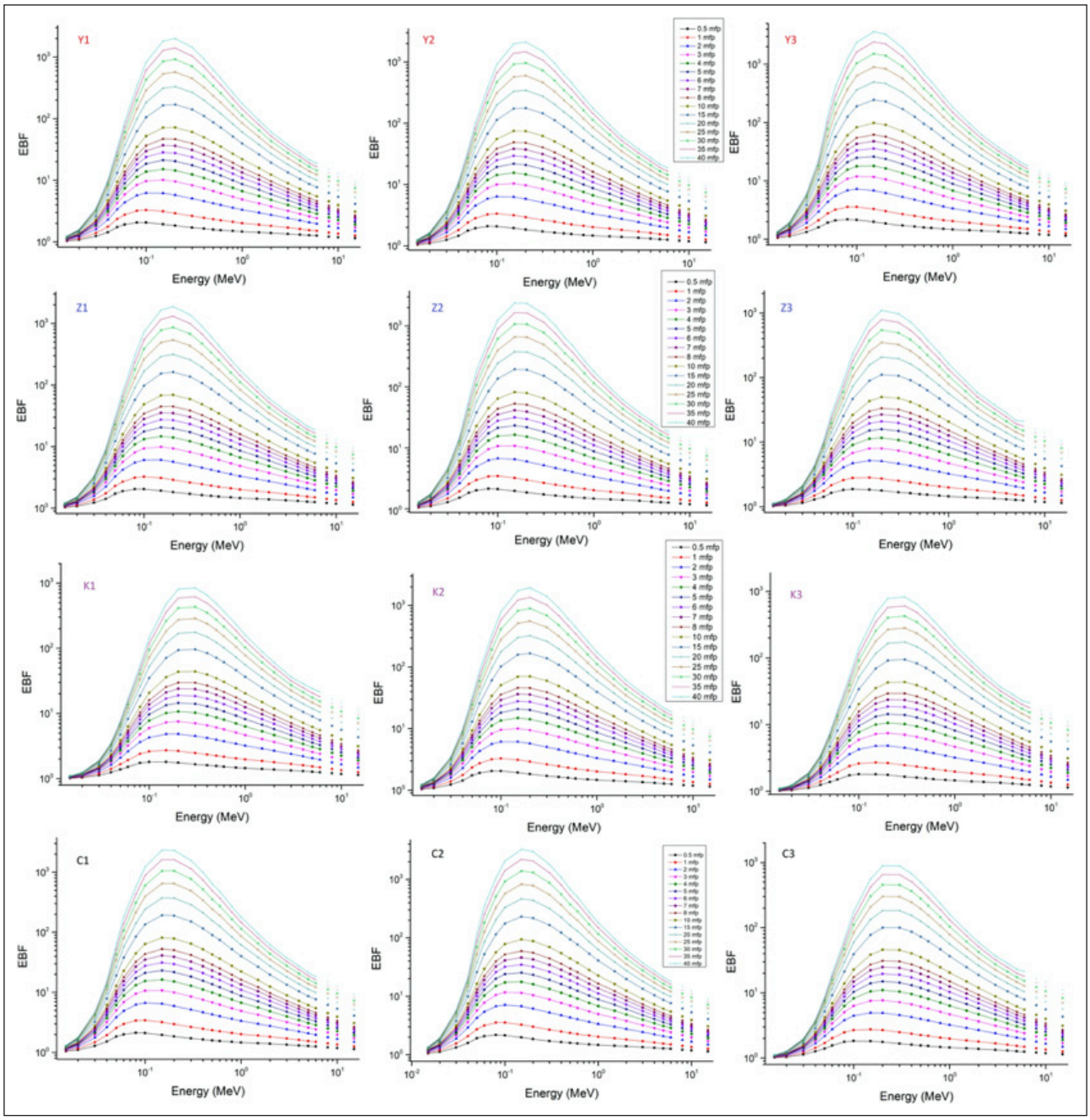

Figure 9. The changes of EBF of the samples versus photon energies.

CONCLUSION

The purpose for performing the study was to produce new materials with higher RSP and good structural properties convenient for applications. In line with this aim, spectroscopic features and RSP of four groups of samples consisting of waste materials were examined by experimentally and theoretically with Phy-X/PSD code. By the help of XRD patterns, the Debye-Scherer equation was used for the crystallite size determination of the samples. Sharp peaks show the high crystallinity properties of the samples. The existence of calcite main phase peaks as well as SiO_2 and cellulose phases were observed by XRD. Mn^{+2} sextets with five weak doublets ascribed to the forbidden transition lines of Mn^{+2} and a singlet assigned to a carbon centered radical with a g value of

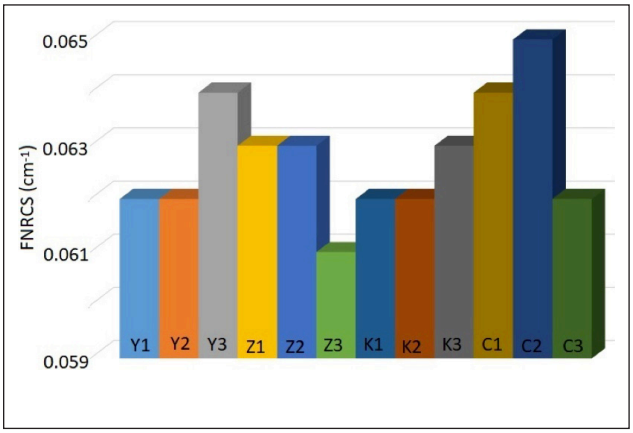

Figure 10. FNRCS values of the samples versus photon energies.

≈2.00 were recorded by EPR. The evaluation of the RSP of the samples were made by obtaining photon-matter interaction parameters by Phy-X/PSD and XCom codes. More shielding properties are observed for K1 (RC(20%)-ESW(60%)-BSW(20%)), K3 (RC(60%)-ESW(20%)-BSW(20%)), C3 (RC(60%)-ESW(20%)-WSW(20%)) and Z3 (GC(60%)-ESW(20%)-BSW(20%)), and lower RSP are found for Z2, C2, C1 and Y3. It is concluded that FNRCS value is the highest for C2 and that is the lowest for Z3. In order to reuse and recycle wastes, it can be recommended that all samples examined with good protection performance can be used as substitute materials instead of cement or aggregate.

ACKNOWLEDGEMENTS

Authors acknowledge the financial support of Bitlis Eren University Scientific Research Projects Coordination Unit (BEBAP) with a project grant number 2023.14. Experimental results were obtained from Advanced Technology Research & Application Center (ILTEK) of Selcuk University.

DATA AVAILABILITY STATEMENT

The author confirm that the data that supports the findings of this study are available within the article. Raw data that support the finding of this study are available from the corresponding author, upon reasonable request.

CONFLICT OF INTEREST

The author declared no potential conflicts of interest with respect to the research, authorship, and/or publication of this article.

USE OF AI FOR WRITING ASSISTANCE

Not declared.

ETHICS

There are no ethical issues with the publication of this manuscript.

REFERENCES

[1] M. S. Nasr, A. A. Shubbar, Z. A. R. Abed, and M. S. Ibrahim "Properties of eco-friendly cement mortar recycled materials from different sources," Journal of Building Engineering, Vol. 31, Article 101444, 2020. [CrossRef]

[2] Z. He, A. Shen, H. Wu, W. Wang, L. Wang, C. Yao, and J. Wu, "Research progress on recycled clay brick waste as an alternative to cement for sustainable construction materials," Construction Building Material, Vol. 274, Article 122113, 2021. [CrossRef]

[3] N. Sathiparan, and H. T. S. M. De Zoysa, "The effects of using agricultural waste as partial substitute for sand in cement blocks," Journal of Building Engineering, Vol. 19, pp. 216–227, 2018. [CrossRef]

[4] S. F. Olukotun, S. T. Gbenu, F. I. Ibitoye, O. F. Oladejo, H. O. Shittu, M. K. Fasasi, and F. A. Balogun, "Investigation of gamma radiation shielding capability of two clay materials," Nuclear Engineering and Technology, Vol. 50(6) pp.957–962, 2018. [CrossRef]

[5] N. F. N. Zuhairi, H. N. Mohd, A. Ripin, M. I. Idris, and N. A. Mohd Radzali, "Study on clay bentonite and kaoline as shielding material," Sains Malaysiana Vol. 49(3), pp. 683–691, 2020. [CrossRef]

[6] I. Akkurt, A. Alomari, M. Y. Imamoglu, and I. Ekmekçi, "Medical radiation shielding in terms of effective atomic numbers and electron densities of some glasses," Radiation Physics and Chemistry, Vol. 206, pp. 1–5, 2023. [CrossRef]

[7] B. Alım, A" comprehensive study on radiation shielding characteristics of Tin-Silver, Manganin-R, Hastelloy-B, Hastelloy-X and Dilver-P alloy's, Applied Physics A, Vol. 126, pp. 262, 2020. [CrossRef]

[8] O. Agar, H.O. Tekin, M. I. Sayyed, M. E. Korkmaz, O. Culfa, and C. Ertugay, "Experimental investigation of photon attenuation behaviors for concretes including natural perlite mineral," Results in Physics, Vol. 12, pp. 237–243, 2019. [CrossRef]

[9] Z. Aygun, M. Aygun, and N. Yarbasi, "A study on radiation shielding potentials of green and red clayey soils in Turkey reinforced with marble dust and waste tire," Journal of New Results in Science, Vol. 10, pp. 46–59, 2021. [CrossRef]

[10] Z. Aygun, N. Yarbasi, and M. Aygun, "Spectroscopic and radiation shielding features of Nemrut, Pasinler, Sarıkamıs and Ikizdere obsidians in Turkey: Experi-mental and theoretical stud," Ceramics Internation-al, Vol. 47(24), pp. 34207–34217, 2021. [CrossRef]

[11] Z. Aygun, and M. Aygun, "A study on usability of Ahlat ignimbrites and pumice as radiation shielding materials, by using EpiXS code," International Journal of Environmental Science and Technology, Vol. 19, pp. 5675–5688, 2022.

[12] M. Aygun, and Z. Aygun, "A comprehensive anal-ysis on radiation shielding characteristics of boro-gypsum (boron waste) by Phy-X/PSD code," Revis-ta Mexicana de Física, Vol. 69(4), Article 040401, 2023. [CrossRef]

[13] M. I. Sayyed, "The Impact of Chemical Composition, Density and Thickness on the Radiation Shielding Properties of CaO–Al2O3–SiO2 Glasses," Silicon, Vol. 15 pp. 7917–7926, 2023. [CrossRef]

[14] H. M. H. Zakaly, H. A. Saudi, H. O. Tekin, M. Rashad, A. M. Shams, Y. S. Issa, A. I. Rammah, M. M. Elazaka, and H. A. Ene, "Glass fabrication using ceramic and porcelain recycled waste and lithium niobate: physical, structural, optical and nuclear radiation attenuation properties," Journal of Material Research Technology, Vol. 15, pp. 4074–4085, 2021. [CrossRef]

[15] B. Oruncak, "Computation of neutron coefficients for B2O3 reinforced composite," International Journal of Computational and Experimental Science and Engineering, Vol. 9, pp. 50–53, 2023. [CrossRef]

[16] R. D. Malidarre, H. O. Tekin, K. Günoğlu, and H. Akyıldırım, "Assessment of gamma ray shielding properties for skin," International Journal of Computational and Experimental Science and Engineering, Vol. 9, pp. 6–10, 2023. [CrossRef]

[17] Q. A. A. D. Rwashdi, F. Q. Waheed, K. Günoğlu, and İ. Akkurt, "Experimental testing of the radiation shielding properties for steel," International Journal of Computational and Experimental Science and Engineering Vol. 8(3), pp. 74-76, 2022.

[18] Z. Aygun, and M. Aygun, "An analysis on radiation protection abilities of different colored obsidians," International Journal of Computational and Experimental Science and Engineering, Vol. 9, pp. 170–176, 2023. [CrossRef]

[19] E. Sakar, O. F Ozpolat, B. Alım, M. I. Sayyed, and M. Kurudirek, "Phy-X / PSD: Development of a user friendly online software for calculation of parameters relevant to radiation shielding and dosimetry," Radiation Physics and Chemistry, Vol. 166, Article 108496, 2020. [CrossRef]

[20] C. Xiang, E. H. Han, Z. M. Zhang, H. M. Fu, J. Q. Wang, H.F. Zhang, and G. D. Hu, "Design of single-phase high-entropy alloys composed of low thermal neutron absorption cross-section elements for nuclear power plant application," Intermetallic, Vol. 104, pp. 143–153, 2019. [CrossRef]

[21] D. F. Jackson, and D. J. Hawkes, "X-ray attenuation coefficients of elements and mixtures," Physics Re-ports, Vol. 70, pp. 169–233, 1981. [CrossRef]

[22] Y. Harima, Y. Sakamoto, S. Tanaka, and M. Kawai, "Validity of geometric progression formula in approximating gamma-ray buildup factors," Nuclear Science and Engineering, Vol. 94, pp. 24–35, 1986. [CrossRef]

[23] Y. Harima, "An historical review and current status of buildup factor calculations and applications," Radiation Physics and Chemistry, Vol. 41, pp. 631–672, 1993. [CrossRef]

[24] ANSI/ANS 6.4.3, "Gamma-ray Attenuation Coefficients and Buildup Factors for Engineering Materials," American Nucl Soc, La Grange Park, Illinois, 1991.

[25] Z. Aygun, "Application of spectroscopic techniques for antioxidant property analysis of various food supplements and ganoderma lucidum coffee," Pakistan Journal of Science Industrial Research B: Biological Scince, Vol. 60(3), pp. 145–153, 2017. [CrossRef]

[26] M. S. El-Mahllawy, A. M. Kandeel, M. L. Abdel Latif, and A. M. El Nagar, "The feasibility of using marble cutting waste in a sustainable building clay industry," Recycling Vol. 3, Article 39, 2018. [CrossRef]

[27] T. Thriveni, S.Y. Nam, J.W. Ahn, "Enhancement of arsenic removal efficiency from mining waste water by accelerated carbonation," IMPC, 2014.

[28] B. Yu, G. Fan, S. Zhao, Y. Lu, Q. He, Q, Cheng, J. Yan, B. Chai, and G. Song, "Simultaneous isolation of cellulose and lignin from wheat straw and catalytic conversion to valuable chemical products," Applied Biology and Chemistry, Vol. 64, Article 15, 2021. [CrossRef]

[29] P. Scherrer, "Bestimmung der Grösse und der inneren Struktur von Kolloidteilchen mittels Röntgenstrahlen," Nachr Ges Wiss Göttingen, Vol. 26, pp. 98–100, 1918. [Deutsch]

[30] M. Aygun, Z. Aygun, and E. Ercan, "Radiation protection efficiency of newly produced W-based alloys: Experimental and computational study," Radiation Physics and Chemistry, Vol. 212, Article 111147, 2023. [CrossRef]

[31] Y. Shimoyama, M. Ukai, H. Nakamura, "Advanced protocol for the detection of irradiated food by electron spin resonance spectroscopy," Radiation Physics and Chemistry Vol. 76, pp. 1837–1839, 2007. [CrossRef]

[32] Y. Shimoyama, M. Ukai, and H. Nakamura, "ESR detection of wheat flour before and after irradiation," Spectrochimica Acta A, Vol. 63, pp. 888–890, 2006. [CrossRef]

[33] M. Ukai, H. Kameya, H. Nakamura, Y. Shimoyam, "An electron spin resonance study of dry vegetables before and after irradiation," Spectrochimica Acta A, Vol. 69, pp. 1417–1422, 2008. [CrossRef]

[34] M. J. Berger, and J. H. Hubbell, "XCOM: Photon Cross Sections Database," Web Version 1.2. National Institute of Standards and Technology Gaithersburg, MD. 20899 USA 1987. [CrossRef]

[35] Z. Aygun, and M. Aygun, "Radiation shielding potentials of rene alloys by Phy-X/PSD code," Acta Physica Polonica A, Vol. 5(141), pp. 507–515, 2022. [CrossRef]